Acta Geotechnica (2019) 14:749–765
https://doi.org/10.1007/s11440-019-00787-w

RESEARCH PAPER

Experimental investigation of microstructural changes in soils eroded by suffusion using X-ray tomography

Cong Doan Nguyen[1] · Nadia Benahmed[1] · Edward Andò[2] · Luc Sibille[2] · Pierre Philippe[1]

Received: 3 July 2018 / Accepted: 10 February 2019 / Published online: 6 March 2019

Abstract
Internal erosion is a complex phenomenon which represents one of the main risks to the safety of earthen hydraulic structures such as embankment dams, dikes or levees. Its occurrence may cause instability and failure of these structures with consequences that can be dramatic. The specific mode of erosion by suffusion is the one characterized by seepage flow-induced erosion, and the subsequent migration of the finest soil particles through the surrounding soil matrix mostly constituted of large grains. Such a phenomenon can lead to a modification of the initial microstructure and, hence, to a change in the physical, hydraulic and mechanical properties of the soil. A direct comparison of the mechanical behaviour of soil before and after erosion is often used to investigate the impact of internal erosion on soil strength (shear strength at peak and critical state) using triaxial tests. However, the obtained results are somehow contradictory, as for instance in Chang's study (Chang and Zhang in Geotech Test J 34(6):579–589, 2011), where it is concluded that the drained strength of eroded soil decreases compared to non-eroded soil, while both Xiao and Shwiyhat (Geotech Test J 35(6):890–900, 2012) and Ke and Takahashi (Geotech Test J 37(2):347–364, 2014) have come to the opposite conclusion. A plausible explanation of these contradictions might be attributed to the rather heterogeneous nature of the suffusion process and to the way the coarse and fine grains are rearranged afterwards leading to a heterogeneous soil structure, a point that, for now, is not taken into account, nor even mentioned, in the existing analyses. In the present study, X-ray computed tomography (X-ray CT) is used to follow the microstructure evolution of a granular soil during a suffusion test, and, therefore, to capture the induced microstructural changes. The images obtained from X-ray CT reveal indeed that fine particles erosion is obviously not homogeneous, highlighting the existence of preferential flow paths that lead to a heterogeneous sample in terms of fine particles, void ratio and inter-granular void ratio distribution.

Keywords Heterogeneity · Internal erosion · Microstructure · Suffusion · X-ray computed tomography

1 Introduction

Internal erosion of soil induced by seepage flow is considered as the main cause of degradation and failure of earthen structures (dikes, earth dams, etc.). It is assumed that four types of erosional processes can be encountered during the internal erosion of water-retaining structures or their foundations: suffusion, backward erosion, contact erosion and concentrated leak erosion [4, 9]. They are all related to intense seepage flow within the earthen structure. In the case of suffusion that is in the scope of the present study, the smallest soil particles are detached and transported by the interstitial water flow through the surrounding soil matrix, mostly constituted of large grains. The strength of the seepage flow and the nature of the materials jointly determine the vulnerability against suffusion within a given embankment dam or dike section. Worrying vulnerability is observed under the following conditions: first, high enough seepage forces are needed, providing sufficient energy and momentum to detach particles from the soil structure; second, the eroded particles should have the possibility to be substantially transported within the porous material by the water flow, which requires the detached

✉ Nadia Benahmed
nadia.benahmed@irstea.fr

[1] Irstea, Aix Marseille Univ, RECOVER, 3275 route de Cézanne CS 40061, 13182 Aix-en-Provence Cedex 5, France

[2] University Grenoble Alpes, CNRS, Grenoble INP, 3SR, 38000 Grenoble, France

particle sizes to be mostly smaller than the ones of the constrictions between the coarser particles of the soil's skeleton. Soils vulnerable to suffusion are denominated as "internally unstable" [20, 23, 35].

The internal erosion potential of different soils has been investigated experimentally by a number of researchers. The related results give an indication about the vulnerability of soils with respect to suffusion in terms of empirical rules that can be prescribed by the particles' size distribution curve [20, 22, 33], the constrictions size distribution [17, 29, 31], the particle shape [25], the effective stress [2, 27] and the hydraulic gradient [32].

The direct observation of suffusion phenomenon is the loss of fine particles and the settlement during the suffusion test. These changes generally lead to an increase in the porosity and possibly a decrease in sample volume of the soil sample [6, 28, 36]. Besides, the coarse grains may rearrange, possibly under fluid flow stresses, but above all, due to the progressive disappearance of the stabilizing presence of fine particles. The initial soil fabric may thus be changed during suffusion process with a possible impact on the subsequent mechanical behaviour.

Changes in the mechanical response of a soil before and after erosion are often used to investigate and quantify the effect of internal erosion on soil strength (shear strength at peak/critical state) using triaxial tests. Chang and Zhang [6] first found that the drained soil strength decreases after the erosion, whereas Xiao and Shwiyhat [36] and later Ke and Takahashi [19] showed that the undrained peak deviator stress of eroded soil is larger than the soil without erosion. As pointed out, the results from these previous experimental investigations on the mechanical consequences of internal erosion are somewhat contradictory. The potential reasons for this might be related to the rather heterogeneous nature of the suffusion process and to the change in soil fabric resulting from selective suffusion [15]. However, the suffusion test results in the literature give only a macroscopic point of view and fail to quantify the suffusion phenomenon at the scale of the soil's induced heterogeneities. Yet, suffusion is precisely expected to initiate at some specific locations where preferential flows occur and then to progress over a certain area within the soil sample as illustrated in Fig. 1 regarding a typical experiment of the present study to be detailed hereafter. The same kinds of transverse heterogeneities (i.e. perpendicular to the main fluid flow direction) induced by suffusion were also observed by Sail et al. [30], Luo et al. [24] and Israr et al. [18]. In addition, longitudinal heterogeneities (i.e. in the direction of the flow) within a soil specimen subject to a suffusion test under constant flow rate are strongly suspected from measurements of the overall hydraulic gradient along the specimen. Rather sharp increases or decreases of the global hydraulic gradient versus time are often observed and were attributed to clogging and subsequent washout of fine particle in some area of the sample, which thus appear as heterogeneities in the direction of flow [19, 24]. Thus, particle-scale analyses of eroded soil are necessary to reveal the microstructural change induced by suffusion and further relate it to the soil's mechanical behaviour. However, few experimental investigations into the suffusion process at this local scale have been reported in the literature [3, 26], and this is the main motivation of the present study.

In this paper, microscopic observations of a soil sample during a suffusion test are investigated by using X-ray tomography with the aim of better understanding the suffusion consequences. The methodology for in-operando X-ray tomography during a suffusion test is firstly presented in Sect. 2. Next, the image processing techniques used to extract microscale measurements from the 3D-reconstituted images are detailed in Sect. 3. Then, the evolution of these microscale measurements during the suffusion development is interpreted in Sect. 4 in terms of void ratio, inter-granular void ratio, fines content and deformation fields. Finally, Sect. 5 summarizes the main outcomes of this study.

2 Microscopic investigation of suffusion development

2.1 Tested materials

In this study, a gap-graded soil is created by using a mixture of two different types of Hostun sands, namely HN 1/2.5 and HN34, which are granular siliceous materials with an angular-to-sub-angular grain shape. The HN 1/2.5 is the coarse fraction grains, while the HN34 sand is considered as the erodible fine particles. These fine particles were used in a proportion of 25% in mass or, equivalently, 25% in solid volume to form the mixture, named FC25.

It is worth noting that suffusion usually occurs in gap-graded granular soils due to their deficiency at certain grain sizes [32]. The potential of suffusion is controlled by the geometric properties of the soil's composition following the methods proposed by Kézdi [22], Kenney and Lau [20, 21] and Burenkova [5], among others. According to these criteria regarding suffusion occurrence, the reconstituted soil is indeed potentially unstable and vulnerable to internal erosion under seepage flow. The properties of these two sands are shown in Table 1, while Fig. 2 provides their grain size distributions together with the one of the mixture.

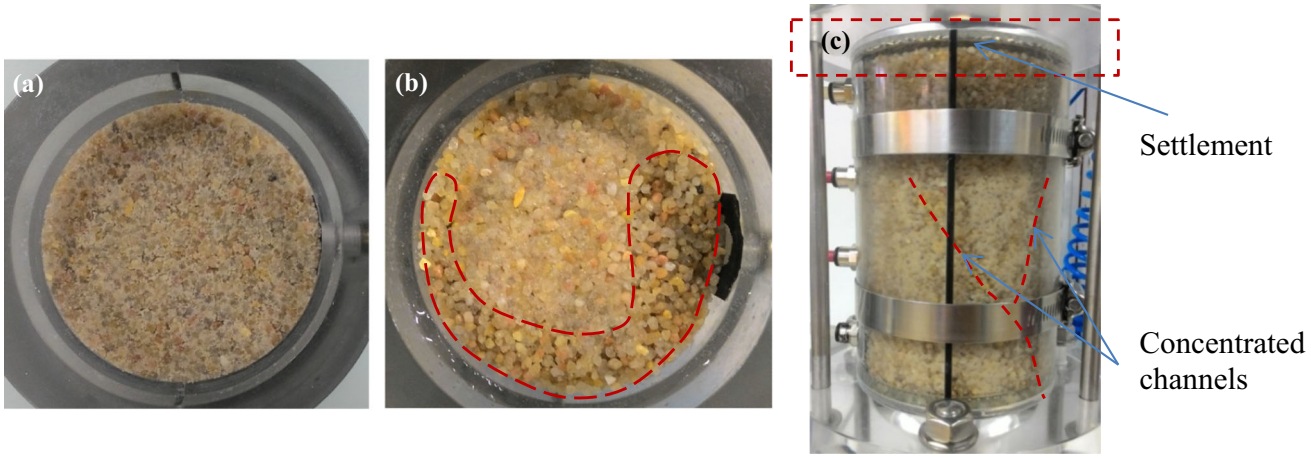

Fig. 1 Photography of suffusion process; **a** initial state; **b** high erosion zone (dash line); **c** concentrated channels of fines migration

Table 1 Sand particles size distribution parameters

Properties	HN 34	HN 1/2.5	FC25
Specific gravity, ρ_s	2.65	2.65	2.65
Minimum particle size D_0 (mm)	0.1	0.63	0.1
Maximum particle size D_{100} (mm)	0.5	2.5	2.5
Median particle size, D_{50} (mm)	0.21	1.7	1.6
D'_{15}/d'_{85}	–	–	5
$(H/F)_{min}$	–	–	0.12
$h' = D_{90}/D_{60}$	–	–	1.24
$h'' = D_{90}/D_{15}$	–	–	9.13

D_X denotes the maximum size of the smallest X% of the soils; D'_{15}: the maximum size of the smallest 15% of the coarse fraction (HN 1/2.5); d'_{85}: the maximum size of the smallest 85% of the fines fraction (HN34); $(H/F)_{min}$: F is the weight fraction of the soil finer than size d and H is the weight fraction of the soil in the size ranging from d to $4d$; $h' = D_{90}/D_{60}$ and $d'' = D_{90}/D_{15}$: conditional factor of uniformity

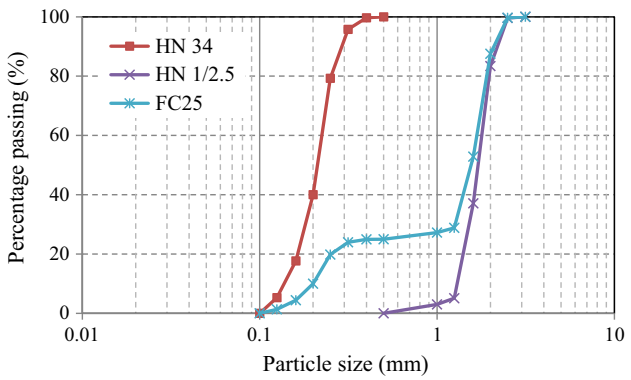

Fig. 2 Particle size distribution curves of the coarse sand (HN 1/2.5), the fine particles (HN34) and the mixture (FC25)

2.2 Suffusion permeameter and specimen preparation

To perform suffusion tests, for understanding the mechanism of this process during which the soil specimen will experience seepage-induced erosion and migration of fine particles, an apparatus called suffusion permeameter was developed and used in this study. The general layout of the apparatus is shown in Fig. 3. It consists of a cylindrical plexiglass cell allowing external visualization of the specimen, fitted with four slots longitudinally for pressure measurements. The inlet of the cell is connected to a Peristaltic Metering pump (FLOWROW N375) which controls the water flow rate through the specimen from a water tank, while the outlet is connected to a soil particle collecting system placed inside the water tank.

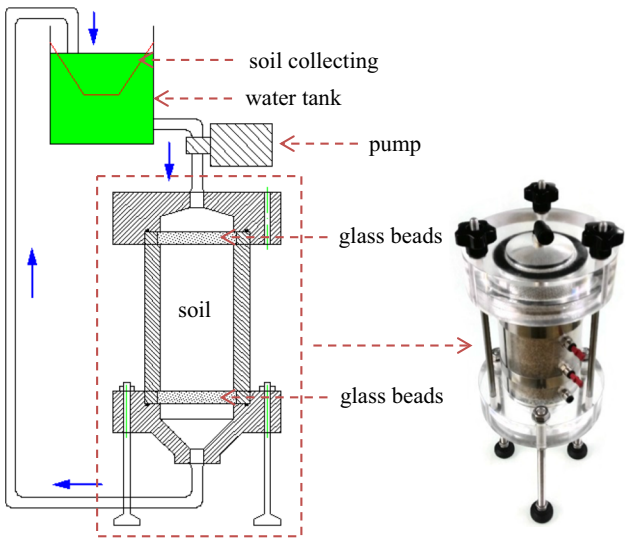

Fig. 3 Schematic diagram of the suffusion permeameter device

The soil specimen is prepared inside the cell by the moist tamping method to prevent soil segregation [1, 11]. Briefly, the soil is compacted in seven successive layers of identical fixed height to reach the target dry density. Each layer represents a seventh of the total soil mass uniformly moistened by a few amount of water (5% in mass), and then compacted manually to the desired height using a graduated tamper. The final dimensions of the specimen are 70 mm in diameter and 140 mm in height. It is placed between two horizontal fixed layers of uniform glass beads (4 mm diameter) of about 12 mm height. These layers help break up the turbulent structures within the incoming flow to ensure an almost uniform and laminar flow through the specimen. Hence, the upper layer does not apply any stress on the sample. To reduce preferential flows between the inner wall and the soil, a rough transparent plastic sheet is beforehand inserted and set against the cell wall.

2.3 Suffusion test with in-operando X-ray tomography

X-ray computed tomography (X-ray CT) aims to quantify a 3D field of X-ray attenuation (a material property linked to density). This is achieved by acquiring radiographic projections of the field under a large number of different angles and reconstructing the 3D field using back projection. 3D field in reality is discretized into 3D volume elements (voxels, a voxel is 3D pixel). The X-ray scan system considered here is able to scan materials with resolutions ranging from a millimetre down to a few micrometres per pixel, depending on specimen size, detector resolution and rotation step size. The full-field measurement provided by X-rays is a revolutionary and increasingly used tool in experimental geomechanics. A spatial resolution greater than 1 mm was firstly used in the study of shear bands in granular soils by Desrues et al. [7]. Later, imaging at particle scale with a resolution of a few microns recently started to be implemented in soil mechanics [12, 13]. Regarding more specifically internal erosion, X-ray CT was used for instance by Homberg et al. [14], Fonseca et al. [10], or more recently Dumberry et al. [8], Bianchi et al. [3] and Mehdizadeh et al. [26].

In the present study, the X-ray scanner in Laboratoire 3SR is used to investigate the consequences of suffusion within a granular sample subjected to an internal erosion test in the X-ray chamber (Fig. 4). The pixel size of the images is 90 µm/px. Compared to the size of the grains constituting the sample, quantified by the median particle sizes of fines d_{50} and of coarse grains D_{50}, the spatial resolution corresponds to $0.43d_{50}$ and $0.053D_{50}$, respectively, which is high enough to visualize individually the coarse grains but not the fine ones.

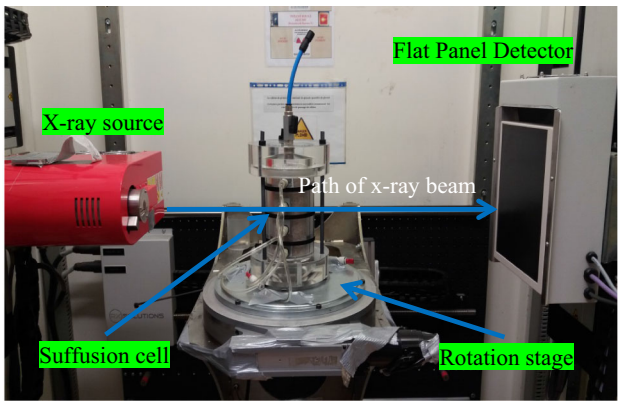

Fig. 4 Set-up of the suffusion cell inside the X-ray chamber

The study of suffusion using tomography being expensive and quite time-consuming, the results presented in this paper concern an observation on a single experiment. Although only one sample was tested in the X-ray tomograph, the experiment carried out was repeated many times out of the tomograph with a good repeatability [16]. This suggests that the rather similar procedure adopted here in the tomography chamber is relevant and leads to the same type of microstructure evolution induced by suffusion.

The specimen preparation is presented in Sect. 2.2. The suffusion test is conducted following a multi-step procedure and is divided into two main phases. The saturation phase consists of circulating carbon dioxide CO_2 through the soil sample from bottom to top (upward direction) under a low pressure gradient, followed by distilled water at a very low flow rate. This step takes approximately 1 h, which appears enough to ensure a good saturation quality since most of the interstitial air is first replaced by CO_2 that next dissolves completely in distilled water.

Afterwards, the erosion phase is launched and consists of applying a downward water flow at a constant flow rate that is progressively increased by steps as illustrated in Fig. 5. The value of flow rate is referred to as the Darcy velocity. The duration of each step is fixed to about 30 min. At the end of each step, an X-ray scan of the sample is performed while the eroded mass is collected and later weighted after drying. Note that the duration and the flow rate of each step were selected on the basis of a preliminary study where the critical flow rate for erosion onset has been identified: a flow rate of 0.15 cm/s was obtained for a similar sample, with same fine content and relative density. In the range of the flow rates investigated, the time for cessation of erosion was always less than 15 min and thus substantially smaller than the step duration. Four scans were performed in the present test, corresponding to four successive soil states during the step-by-step increasing flow rate procedure as depicted in Fig. 5: scan 01 is the scan after the saturation phase; scan 02 is the scan after

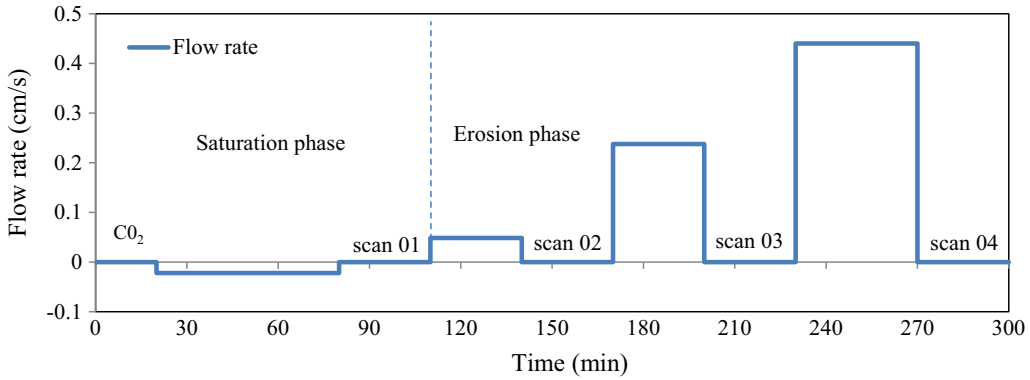

Fig. 5 Application of the flow rate by steps and location in time of the four successive scans

applying a very low flow rate of 0.05 cm/s that is far below the critical flow rate; scan 03 and scan 04 are two scans obtained after the sample had been subjected to erosion with different eroding flow rates and durations. More precisely, scan 03 is performed after the sample was subjected to a flow rate of 0.25 cm/s for 30 min and scan 04 after an additional 30 min loading with a flow rate of 0.45 cm/s. The duration of each scan is approximately 30 min. The remaining masses of fines in the sample during these successive stages of the suffusion test are presented in Table 2. These masses are calculated from the eroded masses in the soil collecting system after drying and weighting. These values will be useful later to assess the subsequent image processing detailed in the next following section.

3 Image processing

The reconstructed 16 bits images of the sample, for a given scan, are in the form of a 3D volume of 900 × 900 × 1700 voxels, corresponding to a physical volume of 81 × 81 × 153 mm. The visualized zone includes the entire soil sample. Figure 6 shows examples of the raw data in a median vertical section. The orientation of the plane is chosen so that it intercepts the most pronounced erosion zone as detailed later. Regarding the reference position of the sample in between two scans, the meridian plane in Fig. 6 is orientated along the X-ray beam direction. Each voxel has a grey level that represents the reconstructed X-ray attenuation at the corresponding point in the sample.

It is worth noting that the movement of fine particles may continue inside the sample after stopping the flow (i.e. during the scanning of the sample); however, the quality of the obtained images, which are very clear, attests that this movement is insignificant (otherwise, the images must be blurry).

In this study, Python programming language and open-source software ImageJ (specifically the Fiji distribution) have been used for image processing and forthcoming analysis. The following steps were successively

Table 2 Volume of fine and coarse grains measured directly by weighting and estimated from image processing, by the end of each phase

	Scan 01	Scan 02	Scan 03	Scan 04
Volume determined by weighing				
Coarse grains (cm^3)	259.7	259.7	259.7	259.7
Fines (cm^3)	85.7	85.7	65.1	39.0
Coarse grains + fines (cm^3)	345.5	345.5	324.9	298.8
Volume determined by image processing				
Coarse grains (cm^3)	259.8	259.7	259.6	259.8
Fines (cm^3)	86.1	85.0	64.3	38.5
Coarse grains + fines (cm^3)	345.9	344.8	323.9	298.4
Sample volume (cm^3)	535.64	535.44	516.08	481.51
Pore[†] (cm^3)	189.69	190.68	194.25	183.93
(pore volume change, cm^3)	(+ 0.0)	(+ 0.99)	(+ 4.75)	(− 5.76)

[†]The true pore volume (= sample volume − volume of fine particles – volume of coarse grains)

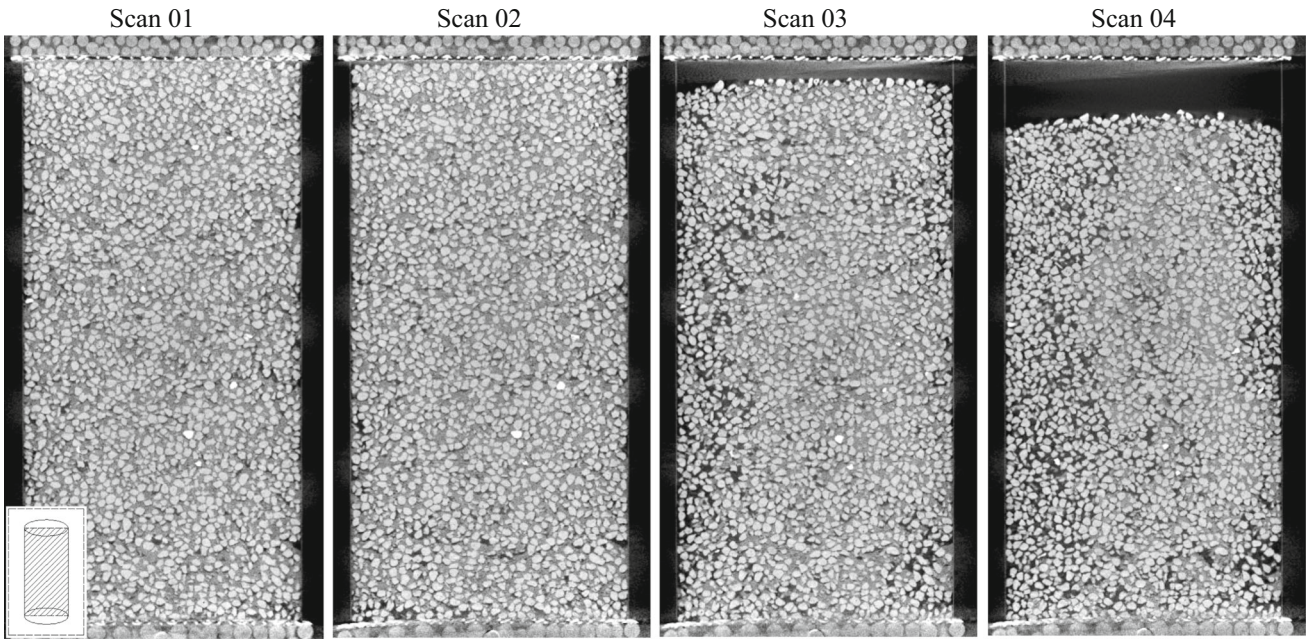

Fig. 6 Vertical sections of the four scans in the median plane of the sample

implemented to post-process the raw 3D reconstructed images obtained from the four X-ray scans.

First, all the volume located outside of the soil sample is removed by imposing a zero grey level. This cleaning is performed manually. From this step, the 3D-reconstructed scan includes only coarse grains, fine particles and voids (pure water) inside the soil sample. Being made of the same material (silica sand), fine and coarse particles should be approximately represented by the same grey level. However, as the size of a fine soil particle is small regarding the spatial resolution (d_{50} = 210 μm; voxel size = $0.43d_{50}$), the grey level of individual fine particles is difficult to measure accurately and only a mean grey level of a mixture of fine particles and inter-fine water can be obtained. This results in an apparent grey level lower than the one corresponding to a pure silica material (coarse grains). Consequently, the average grey-level value of coarse grains and interstitial water remain almost unchanged in the whole sample and are rather easy to determine from a selection of voxels containing exclusively coarse grains or interstitial water, respectively. On the other hand, the grey level of voxels including fine particles depends on the concentration of fine particles in each voxel volume, its value ranging from the mean grey level of water to the mean grey level of silica (coarse grains). The next steps consist in, first, identifying the coarse fraction from the sample and, second, correlating the grey level in the inter-coarse granular space with the fine particles concentration.

By applying a given threshold on the grey levels of the reconstructed image, one gets a binarized image composed of two phases: the inter-granular space and the coarse grains. The voxel volume being known, the total number of voxels included in the coarse granular phase gives a measurement of the volume of coarse grains in the sample. The threshold value is selected to match this coarse grain volume obtained from image processing with the one deduced from the mass of the coarse grains used to make the sample (see Table 2). An example of the resulting binarized images is shown in (Fig. 7b) where coarse grains are displayed in black.

In the second step, the grey level of voxels included in the inter-granular space (identified in the previous step) is rescaled from 0, in order to be representative of the fine concentration in these voxels, according to the mean grey level of pure water and pure silica (i.e. grey level of coarse grains). The rescaling is performed such that the grey level of voxels including only pure water is now equal to 0 and the one of voxels filled with only silica is equal to 1. Then, the rescaled grey level of any voxel including fines and water can be used to quantify the local content in fine particles, strictly comprised between 0 and 1, most values being lower than 0.7. The new images obtained this way are called calibrated images. Nevertheless, to clearly identify the coarse grains in the calibrated images, the masks of the coarse grains obtained from the binarized images are used by superimposition pixel by pixel on the calibrated images. Therefore, calibrated masked images are ultimately obtained where the grey level of all coarse grains voxels is strictly equal to 1, while the grey level of all other voxels varies from 0 (pure water) up to 1, according to the local concentration in fine particles. Figure 7c shows an example of the filling rate of fines particles

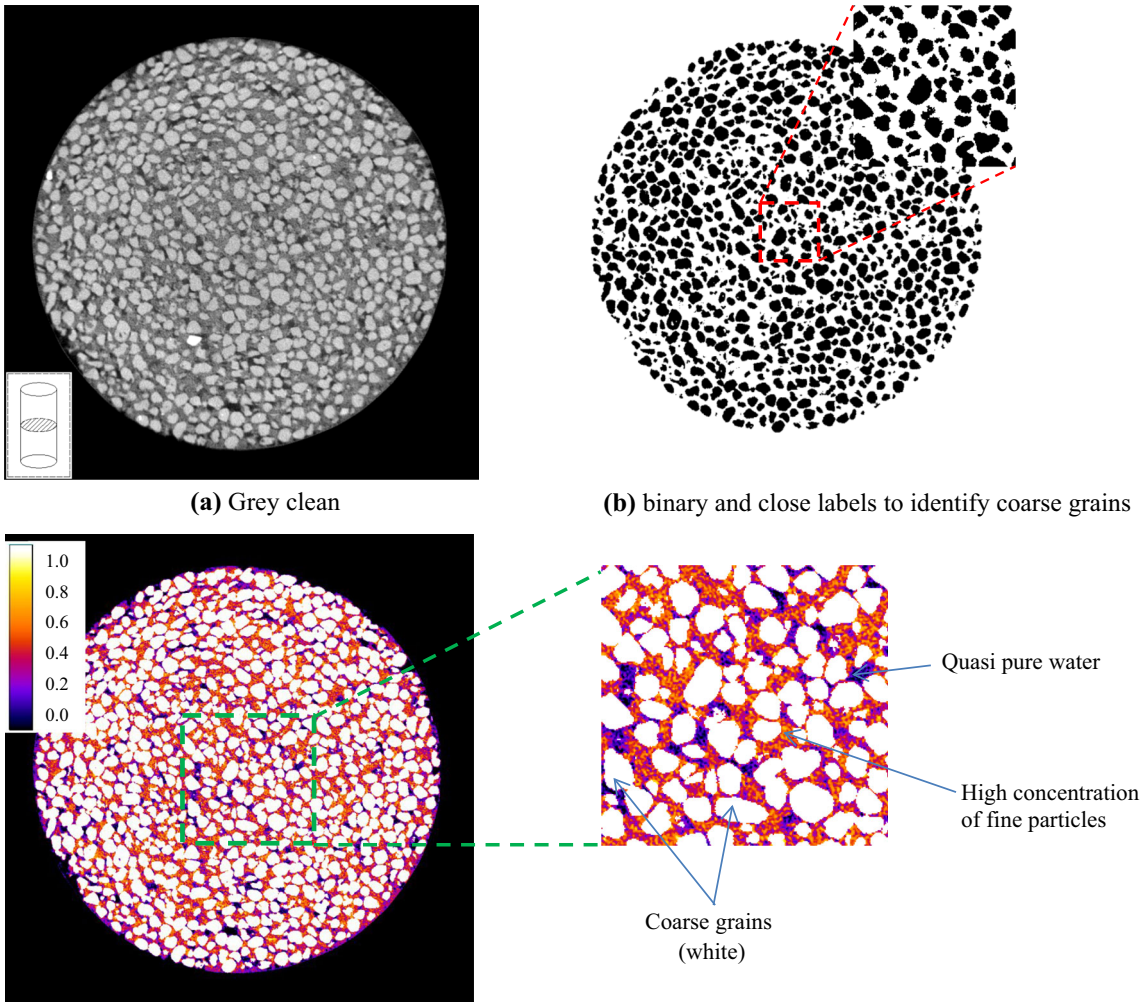

(a) Grey clean

(b) binary and close labels to identify coarse grains

(c) filling rate of fine particles in the pores

Fig. 7 Successive steps for identification of the coarse granular phase and computation of the fine concentration

in the pores obtained in this way. Finally, the fine particles volume can be calculated by the following equation:

$$V_{\mathrm{FP}} = \sum_{\mathrm{voxel} \in \mathrm{inter-granular\ space}} \left(V_{\mathrm{vox}} \times I^{\mathrm{c}}_{\mathrm{vox}}\right)$$

where V_{FP} is fine particles volume; V_{vox} is voxel size (90 µm); $I^{\mathrm{c}}_{\mathrm{vox}}$ is concentration in fine particles of each voxel.

Qualitatively, Fig. 8 shows the vertical section of each sample in the same median plane as the one presented in Fig. 6, using a colour map for the degree of filling of fine particles in the inter-granular pores.

Quantitatively, Table 2 shows the volumes of fine particles and coarse grains computed from the image processing which can be consistently compared to the values directly deduced by weighing. These results validate the ability of the proposed image processing to give local and quantitative information about the microstructure of the sample at the different stages of the suffusion process.

4 Description of suffusion development

From the vertical and horizontal sections (Figs. 8, 9), scan 01 and 02 show that fines loss is not distinguishable except at the bottom part of the sample where a slight change in fine particles concentration is observed. On the scans 03 and 04, the development of suffusion essentially takes place in a vertical channel, along the whole sample height, located at some positions around the lateral sample wall. This development starts around the sample periphery from the top and progress non-uniformly to the bottom part. Such a development might be due to a stronger edge effect on the sample top layer directly in contact with the flow.

Subsequently, the preferential flows are formed in a rather random way, progressing longitudinally and horizontally as illustrated on the scan 03, by the erosion of fine particles which appears less concentrated on the perimeter of the horizontal section in the middle of the sample

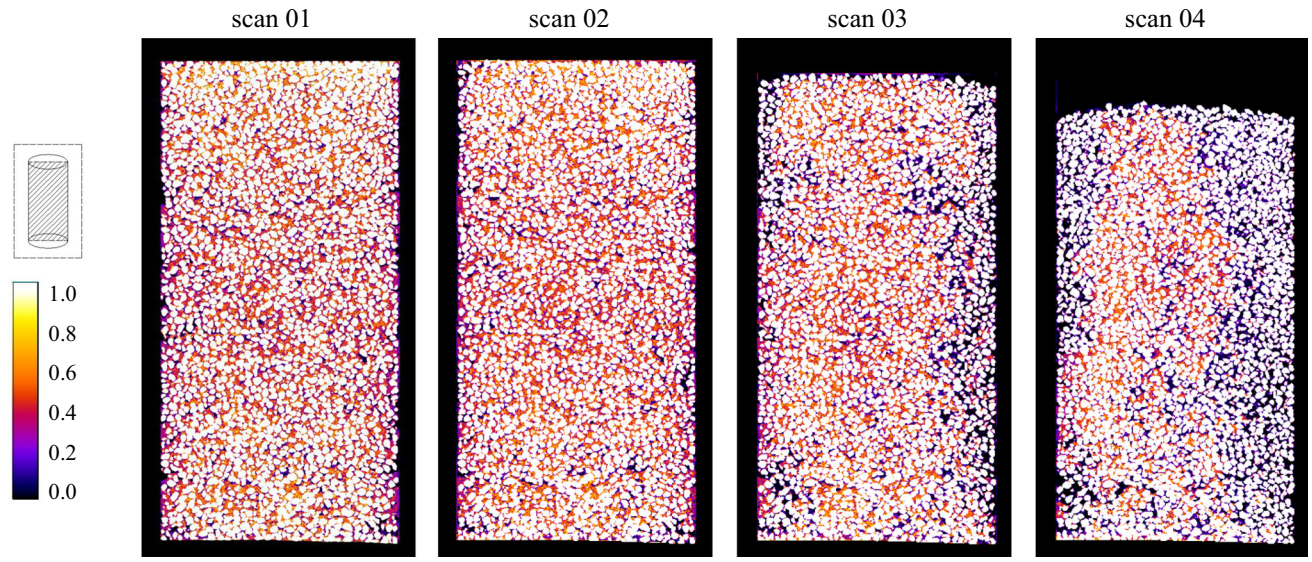

Fig. 8 Vertical sections in the median plane of the four scans after calibration of the fine solid concentration in the inter-granular space

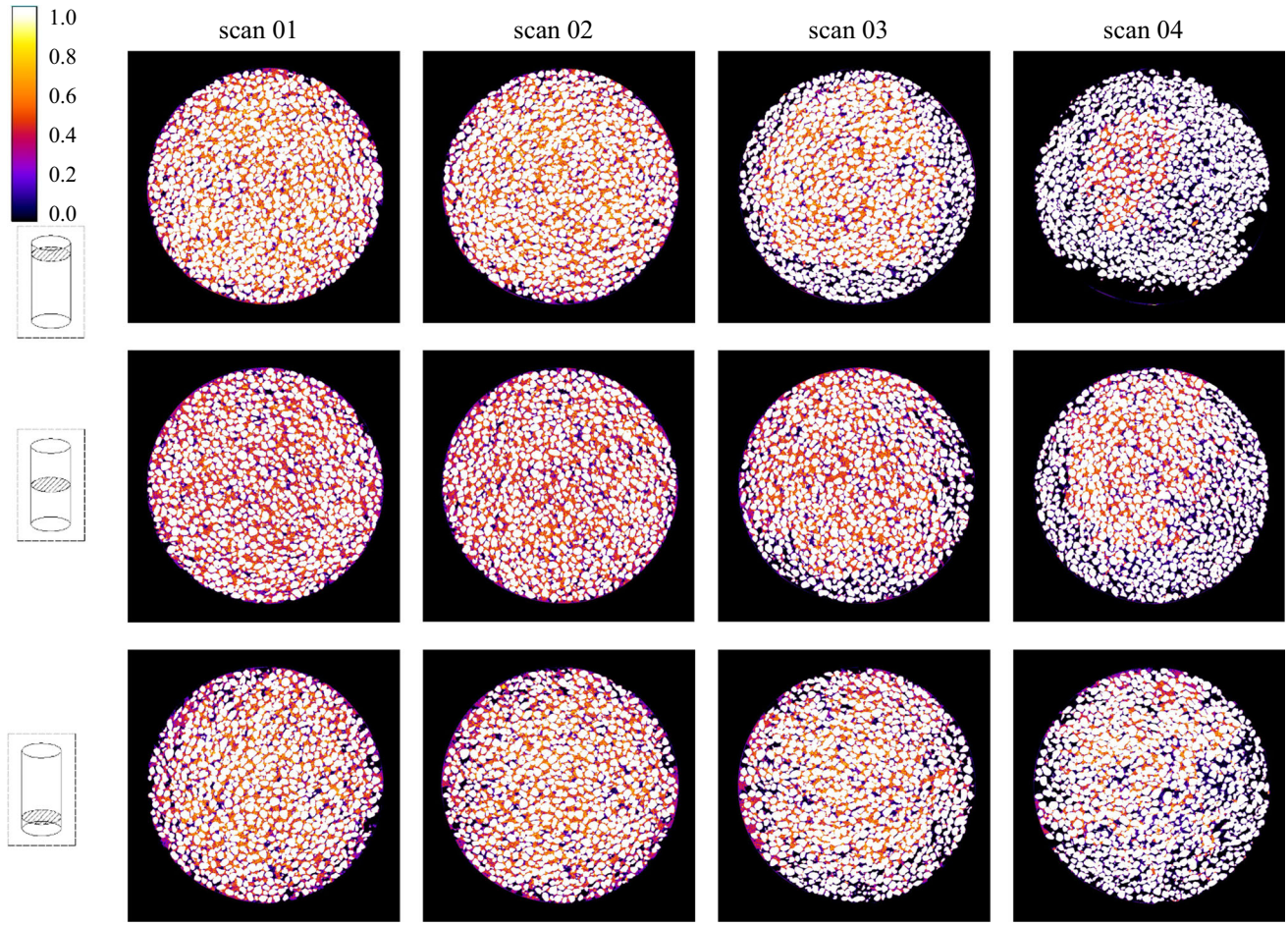

Fig. 9 Horizontal sections of the four scans at three different sample height positions after calibration of the fine solid concentration in the inter-granular space

compared to that of the upper part. On the lower part, the preferential flows seem to converge, inducing a new depletion in fines concentration near the edge of the sample. This observation is more remarkable on the scan 04 when the erosion of fines becomes stronger.

One could notice the appearance of differential settlement induced by the erosion (under its own weight and the impact of downward flow) which is not symmetrical either on the axis or in the plane. This is consistent with the above observation related to the edge effect and the concentrated preferential paths close to the boundary.

5 Results and discussions

5.1 Global change in the sample physical state

The evolution of the state properties (density and fine content) of the sample during the suffusion test is firstly studied at the sample scale. From the results of the images processing detailed in the previous section, the following variables can be directly calculated: (1) the void ratio e that compares "void" volume (i.e. pure water) to solid volume; (2) the inter-granular void ratio e_g that is similar to the void ratio except that fines are now considered as void; (3) the fines content f that compares fine grains volume to total grains volume. These quantities, calculated for each scan for the whole sample, are presented in Fig. 10.

As expected, no visible global change is observed between scan 01 and scan 02 since no erosion in the sense of particles washout has occurred due to the very low flow rate. Then, from scan 02 to scan 04, as the flow rate is increased, the fine content globally decreases with the development of erosion which should lead to a more and more open microstructure. However, the settlement of the sample comes together with the erosion development. Such

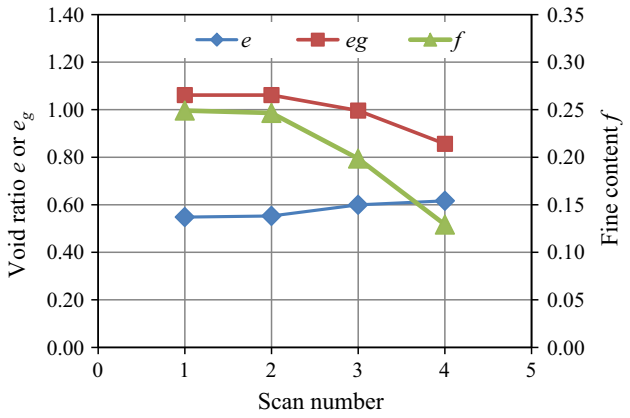

Fig. 10 Void ratio e, inter-granular void ratio e_g and fine content f of the four successive scans

a settlement can be observed via the decreasing of the inter-granular void ratio corresponding to a compaction of the coarse granular skeleton. These two mechanisms are somehow in competition, with a slight predominance of the microstructure opening (due to fine departure) as the global void ratio is eventually slightly higher avec erosion than before (even if the coarse granular phase is itself denser).

By closely examining the change in real pore volume V_v, it can be stated whether erosion of fine particles (i.e. increase in V_v) or granular skeleton settlement following the erosion process (i.e. decrease in V_v) is dominant. In that respect, Table 2 shows that erosion is the main process modifying and loosening the overall sample structure in scan 03. However, in this state, the pore volume is almost unchanged compared to the previous state implying that the increase in V_v by losing fine particles was almost equivalent to the decrease in V_v caused by granular skeleton settlement. In scan 04, even if in this case the erosion is greater than at the previous step, the sample is mainly affected by settlement and densification, resulting probably from an induced metastable skeleton structure. Nevertheless, the sample scale does not allow so far for more thorough analysis of erosion and subsequent settlement. An investigation at a more local scale is necessary as will be detailed in the next section.

5.2 Local state and deformation

From the calibrated images presented previously, the sample can be meshed on a regular lattice to create meso-scale sub-volumes, each sub-volume including several voxels. Such sub-volumes will be used to define and compute local fines content, void ratio and inter-granular void ratio which cannot be defined at the scale of a single voxel (except for the fines content if the voxel belongs to the inter-granular space). The optimal size of the sub-volume is required so as to define a representative elementary volume (REV). For this purpose, the evolution of the inter-granular void ratio in scan 01 has been considered as a function of the mesh size (Fig. 11). The different curves stand for 20 distinct cube centres chosen randomly. The results show that beyond a mesh size of almost 50 px (4.5 mm), the inter-granular void ratio tends to some constant value, irrespective of the chosen sub-volume size. The REV size for this material is consequently around 50 voxels or, equivalently, a little less than three times the median diameter D_{50} of the coarse grains.

Figure 12 shows the spatial fields of the different physical properties (e, e_g and f) of the soil sample during the erosion test in the median vertical plane; each point corresponds to a representative value averaged in a cube of side 50 px, representing 4.5 mm (i.e. the average is also performed in the direction orthogonal to the vertical plane

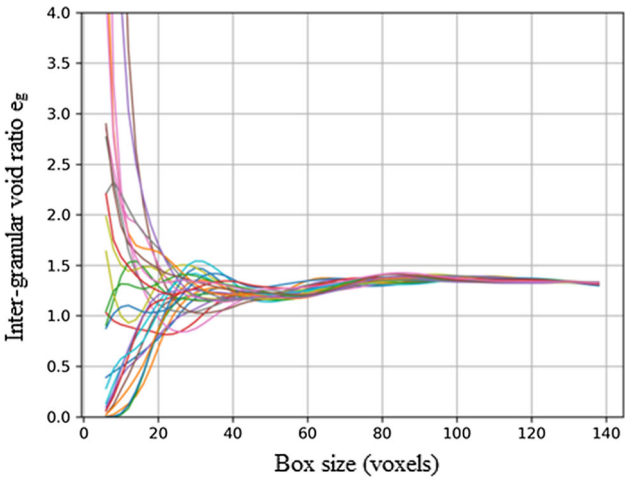

Fig. 11 Inter-granular void ratio versus the box size used for its calculation

shown in Fig. 12 over a length of 50 px). After preparing the sample, scan 01 reveals an almost homogeneous distribution of void ratio e, inter-granular void ratio e_g and fines content f without grain segregation. Besides, the initial homogeneous distribution of fines seems not to be affected by the saturation stage, performed before the first scan. Comparison of scans 01 and 02 confirms also that no noticeable erosion is observed at low flow rate. On the contrary, in scans 03 and 04, where suffusion occurred, there is a significant drop in fines content, especially at the circumferential edges of the sample, indicating that most of the fine particles removal remains mainly located at the periphery of the soil sample. This observation is probably due to edge effects. Despite the use of a rough transparent plastic sheet at the lateral wall (see Sect. 2.1), a rather flat boundary condition subsists for the erosion cell and is responsible for a slightly looser stage of the soil at the vicinity of the lateral wall. This is indeed visible in the distribution of the void ratio e for scans 01 and 02 where both left and right vertical boundaries of the figure are slightly lighter (i.e. looser according to the colour scale) than the sample bulk. Consequently, preferential flow paths are initially present near the cell wall, and they are progressively strengthened as the flow rate increases.

As observed previously at the sample scale, the increase in void ratio is also directly correlated, at the REV scale to the decrease in fines content, although mitigated by an overall settlement of the specimen. Indeed, the void ratio is heterogeneous, but even if at the sample scale, the void ratio globally increases (and the sample becomes looser), it is not true everywhere locally. In the last scan, the sample is looser (i.e. the void ratio e) than initially on the periphery but it is slightly denser in some places in the bulk. On the contrary, the inter-granular void ratio seems only slightly affected by these surrounding preferential flows. Its initial rather homogeneous distribution within the sample remains almost unchanged, showing that erosion induces only an overall decrease in the inter-granular void ratio in the entire sample. A slight heterogeneity appears nonetheless in scan 04.

In the following paragraphs, the reconstructed images are used to perform volumetric Digital Image Correlation (DIC) in order to derive the displacement field and then the deformation fields related to the coarse granular phase. These specific image processing techniques are not described in this paper, but details can be found in Tudisco et al. [34]. The code used here is the SPAM toolkit, currently under development. Inter-granular voids including fines are discarded in the image correlation processing as the displacement of fines may result from erosion process and is not representative, in this case, of the local deformation of the soil. In this objective, the binarized image obtained in the first step of the image processing (Fig. 7b) is used as a mask on the grey-scale image (Fig. 7a) such that voxels (and their grey-level information) corresponding to the coarse grains are the only ones taken into account in the DIC. Incremental deformation fields (deformation fields between scans 01–02, scans 02–03 and scans 03–04) are calculated, and the volumetric strain (first invariant of the strain tensor) and the intensity of the deviatoric strain (proportional to the second strain invariant) are presented in Fig. 13.

On volumetric strains maps, a negative volume deformation (in blue on the images) corresponds to a decrease in volume. As observed here, a significant volume decrease occurs at the periphery of the sample than in the centre. This can be explained by a larger settlement in this zone owing to the rigidity of the cell and on the induced preferential paths at the periphery, as shown previously. This is also consistent with the bulging shape of the upper surface of the sample as shown in Fig. 8. On the increment 03–04, we observe very locally some volume increases (sections a–a and b–b). In some zones, close to the sample boundary, the convergence of the DIC algorithm was not total (because of relatively large displacements of the coarse grains at those places). Therefore, such local zones highly dilatant (associated to neighbouring zone highly contractant) are an artefact of the DIC itself than representative of the actual volume change.

Concerning the incremental deviatoric strain field, it reveals more specifically the presence of shear strain. The shear strain remains at a rather low intensity within the specimen. The local high shear intensity near the sample boundaries (in the same zones as the volume increases) should be discarded from the reasons given here above. Nevertheless, shearing develops in the bulk of the sample. This is consistent with the relatively higher peripheral settlement (compaction) which should accommodate with

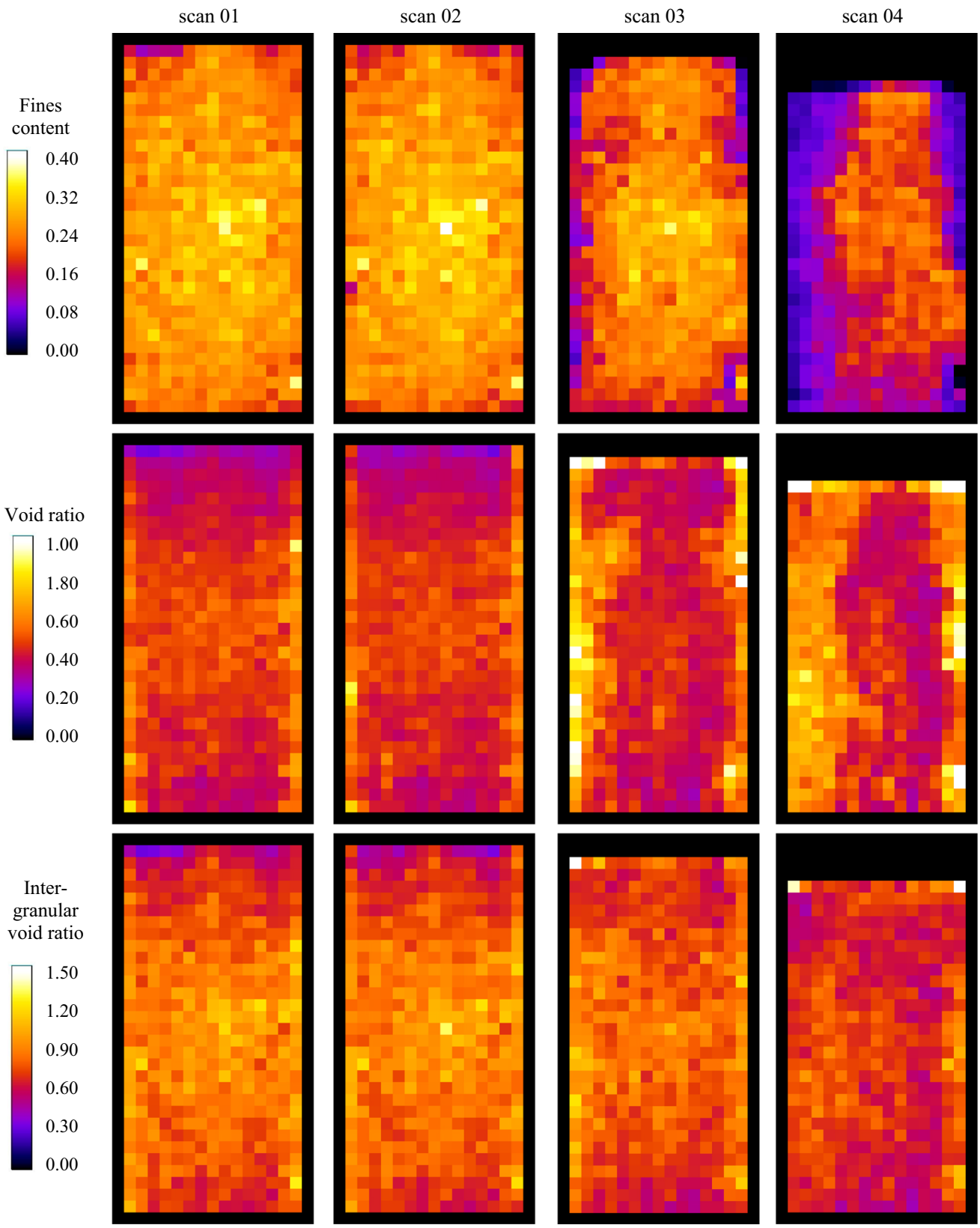

Fig. 12 Fields of fines content, void ratio and inter-granular void ratio in the median vertical plane of the four scans

the lower settlement along the sample axis. In other words, due the heterogeneous development of suffusion, the soil sample does not experience a strict compaction in oedometric conditions but is also slightly sheared under its own weight.

5.3 Vertical profiles of fines content, void ratio and inter-granular void ratio

To obtain further quantitative results on the local physical properties (fines content f, void ratio e and inter-granular void ratio e_g), some space-averaging is implemented. First, all the f, e and $e_{.g.}$ values in voxels located at a given height z are averaged in a horizontal slice of 30 voxels thickness to evaluate $f(z)$, $e(z)$ and $e_g(z)$, respectively. The corresponding vertical profiles of fine contents, void ratio and inter-granular void ratio, as well as the incremental variations of these parameters with respect to the previous scan are presented in Fig. 14.

Interestingly, the interfaces between the compacted layers by moist tamping method (depicted by dotted lines) are clearly visible on the profiles from scan 01 and scan 02, still distinguishable in scan 03 and ultimately disappear in scan 04 due to both the washout of the eroded fine particles

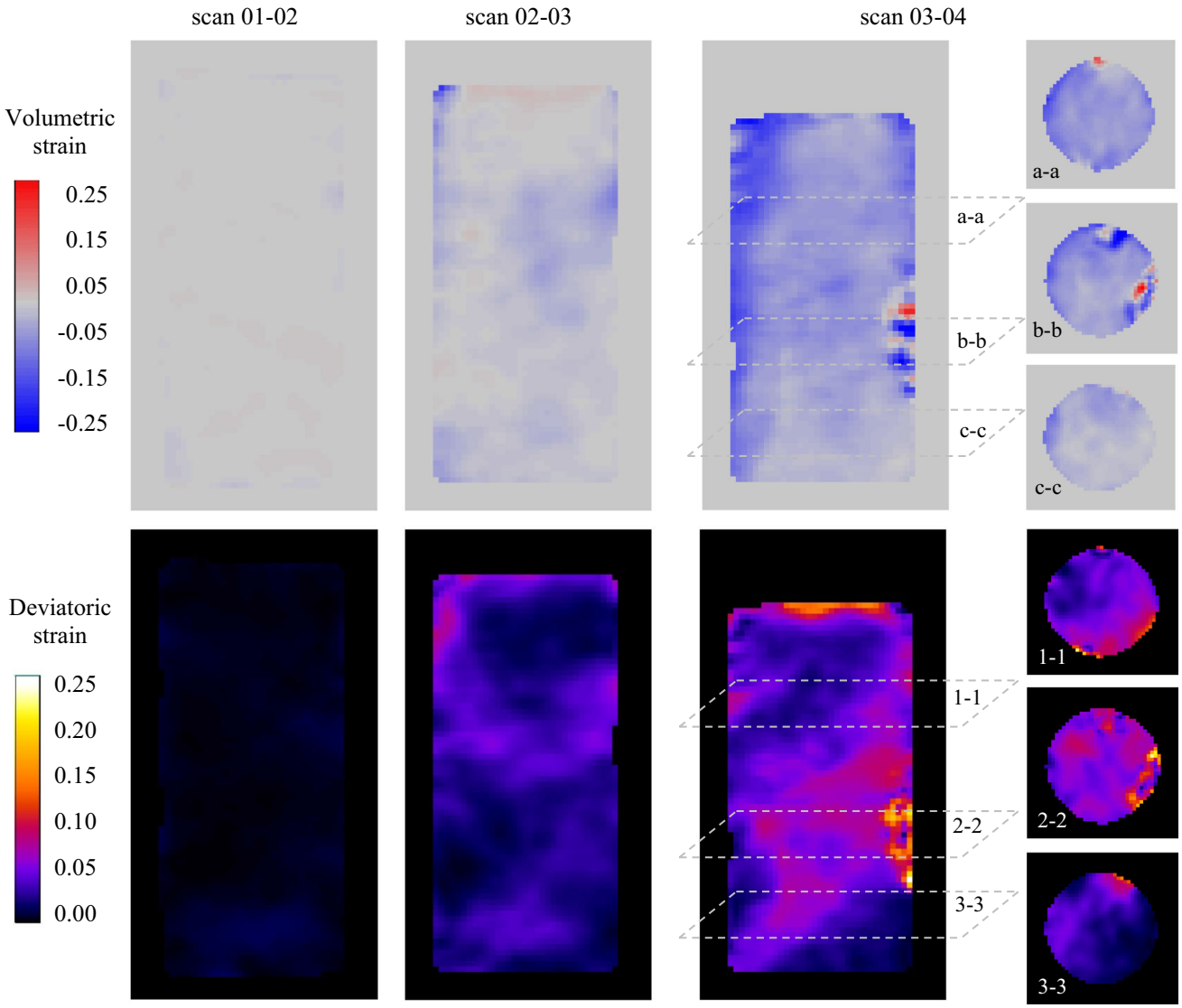

Fig. 13 Map of incremental volumetric and deviatoric strains in the median plane

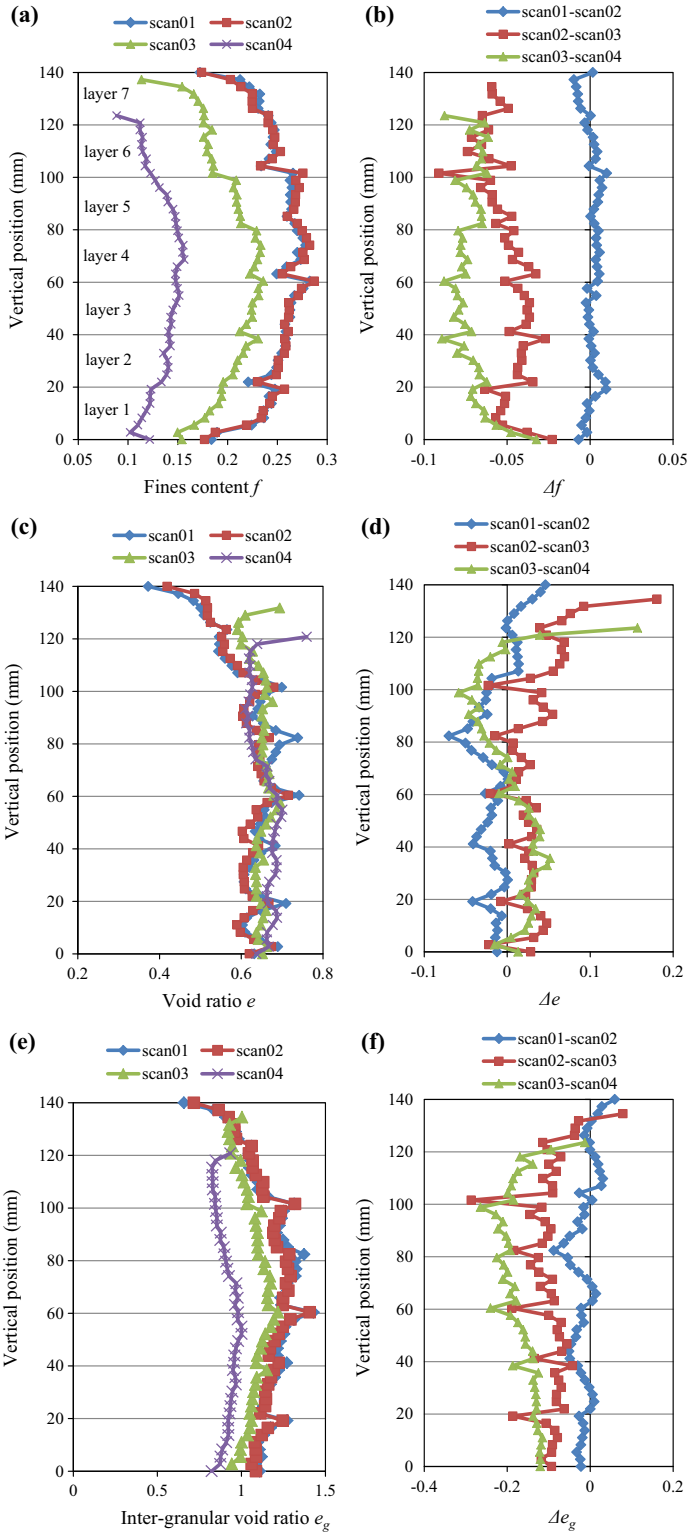

Fig. 14 Vertical profiles of **a** fines content, **b** incremental variations of fines content, **c** void ratio, **d** incremental variations of void ratio, **e** inter-granular void ratio and **f** incremental variations of inter-granular void ratio of the four scans

and the substantial rearrangement of coarse grains. This implies that the sample preparation by moist tamping method does not really create a perfectly homogeneous sample with the obvious presence of layering, as previously demonstrated by Frost and Park [11]. An over-compaction is also observed in the upper layer and, to a lower degree, in the one immediately below. Regarding the fines content (Fig. 14a), there is a substantially smaller concentration in the top and the bottom layers. By analysing the variation of the fines content between scan 01 and scan 02 (Fig. 14b), although it is confirmed that the global amount of fines content remains constant since the washout of the fines particles has not yet occurred in this step, some slight changes in the vertical distribution of the fines particles can be observed nonetheless. The most significant change is a migration of fines at the top of the sample towards the rest of the specimen. To understand this, it is worth recalling that scan 01 and scan 02 are, respectively, obtained after the saturation phase performed with an upward flow and after the phase of the flow reversal (downward) to carry out the erosion stages. Indeed, during the saturation step, fine particles contained between (or surrounding) the coarse grains might fall downward for a certain distance at the wetting front during water infiltration into sample. Afterwards, it is likely that the change in the flow direction can rather easily re-mobilize these particles and consequently slightly modify the fines concentrations with an expected loss at the top of the sample and a general migration downward. From Fig. 14a, scans 03 and 04 are characterized by a significant drop in fines content throughout the entire sample height as erosion occurs, more pronounced in the two upper layers for scan 03 and roughly homogeneous for scan 04, except at the bottom of the sample where a lesser loss of fine particles is observed in both scans.

Regarding the evolution of the void ratio (Fig. 14c), it can be observed that, apart from the top of the sample, the void ratio varies only slightly throughout its height. This is to be attributed to a balance between the erosion of the fine particles and the settlement. Consistently, the inter-granular void ratio decreases more significantly due to the progressive collapse and reorganization of the coarse grains induced by the loss in fines and subsequent localized instabilities (Fig. 14e).

One should note that, with the exception of the discontinuities located at the transition between the different soil layers, there is not much heterogeneity induced by erosion along the vertical direction as shown by all these vertical profiles. Therefore, no local clogging of fine particles (that would be represented by a sharp increase in the fines concentration) was observed in any given horizontal sections.

5.4 Radial profiles of fines content, void ratio and inter-granular void ratio

The physical properties of the soil (fines content f, void ratio e, inter-granular void ratio e_g) are now averaged at a radial distance r from the revolution axis of the sample in the volume between $r - \Delta r/2$ and $r + \Delta r/2$ (with $\Delta r = 30$ pixels). The corresponding radial profiles of $f(r)$, $e(r)$ and $e_g(r)$ and the incremental variations of these parameters with respect to the previous scan are plotted in Fig. 15.

The edge effects and related induced heterogeneities are clearly visible in all these radial profiles, even for scan 01. It can thus be noted that the preparation method, combining moist tamping (compaction control at the periphery) and saturation, fails to create a homogeneous sample in terms of radial distribution. A substantial lack of both fine particles and coarse grains occurs at the lateral wall as revealed by a lower fine content and a higher inter-granular void ratio in scan 01. The evolution from scan 01 to scan 02 of fines content (Fig. 15a) is almost negligible, as expected though the flow rate was too low for erosion to occur. Only slight changes are observed at the lateral wall. In scans 03 and 04, where significant suffusion occurred, the loss in fine particles near the periphery is much higher compared to the one in the centre and there is a rather progressive decrease in f as the radius increases. However, as regards the incremental change in fines content (Fig. 15b), scan 03 reveals a zone at the periphery where a high gradient in fines content increment is observed, whereas it remains almost constant in the central zone. Conversely, scan 04 displays a roughly constant and homogeneous distribution of the incremental change in fines. In other words, erosion of fine is strongly heterogeneous (with respect to the radial direction) in the increment 02–03 and then tends to become homogeneous in the increment 03–04.

Regarding the incremental evolution of the void ratio during erosion (Fig. 15d), it can be interestingly noted that, in the centre of the sample, approximately for $r/R < 0.5$ (R: sample radius), the void ratio is slightly lower; the soil is generally in a slightly denser state. In this zone, the loss of fine appears to be slightly over-compensated by coarse grains settlements. The latter, as shown in the radial profiles of the inter-granular void ratio (Fig. 15e), occurs approximately in the same way everywhere in the sample since a roughly homogeneous decrease in Δe_g along the radial direction is observed.

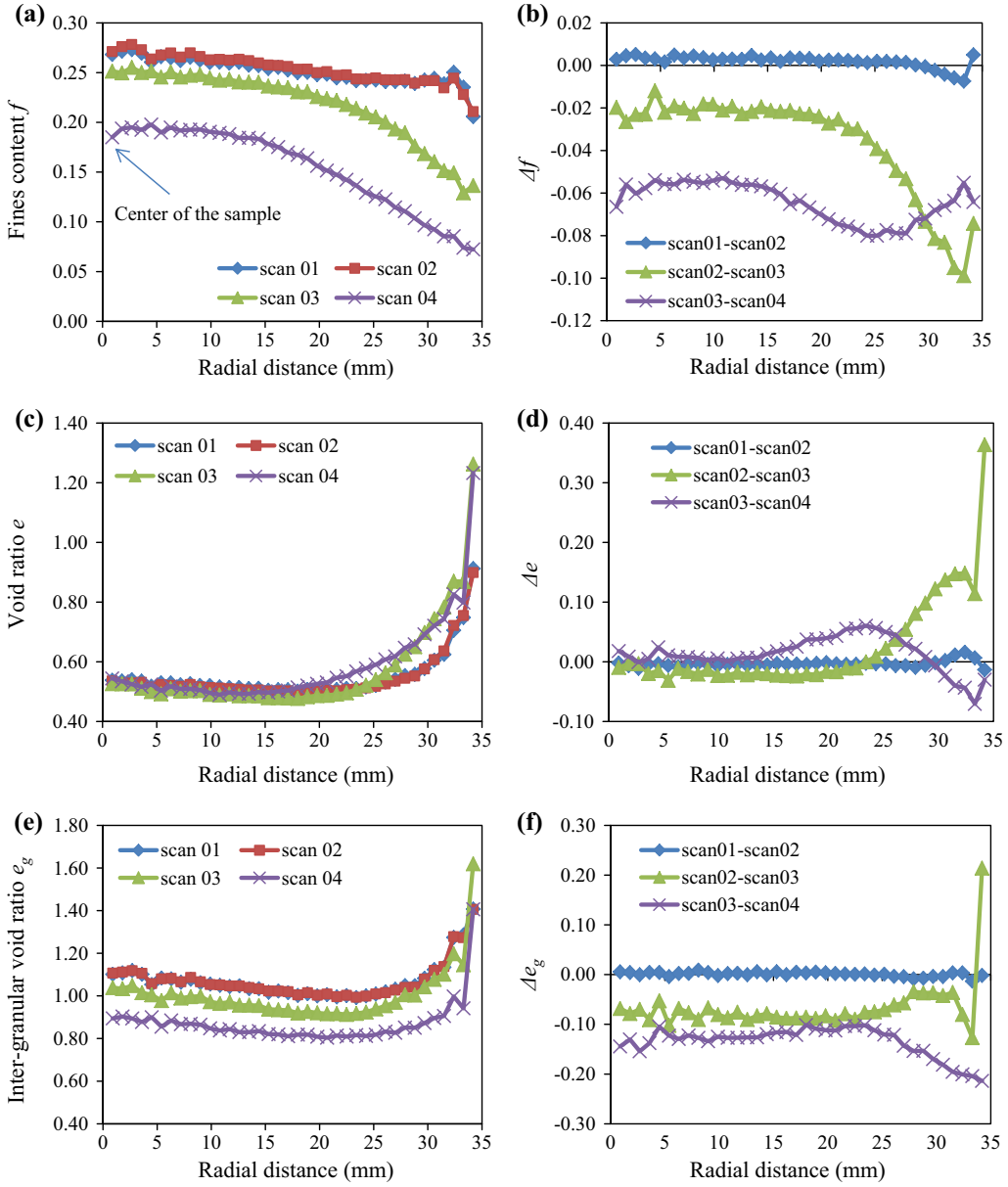

Fig. 15 Radial profiles of **a** fines content, **b** incremental variations of fines content, **c** void ratio, **d** incremental variations of void ratio, **e** inter-granular void ratio and **f** incremental variations of inter-granular void ratio of the four scans

6 Conclusion

In this study, X-ray tomography technique has been used to experimentally characterize the impact of suffusion on the soil microstructure. The microstructural changes during the suffusion process were accurately investigated in terms of strain fields and spatial distribution of fines content, void ratio and inter-granular void ratio through vertical and radial profiles. The following conclusions can be drawn.

From a practical perspective, it was demonstrated here that, for an X-ray CT of a gap-graded soil, a spatial resolution of images around half the median diameter of the fines particles (more precisely here a resolution of $0.43d_{50}$) was sufficient to measure the different physical properties (fines content, void ratio and inter-granular void ratio) with a high accuracy. This conclusion reinforces the potential of using X-ray CT data in complement to numerical results provided by discrete element methods (DEM) for instance and to mechanical tests at macroscale. These data could be very useful for interpreting, in a more objective and coherent manner, the mechanical behaviour of granular soils, especially the altered or destructured ones by erosion or other processes.

A secondary practical outcome of the present study is the confirmation that the moist tamping method fails, in a certain way, to create a reasonably homogeneous sample since it generates a microstructural stratification, in agreement with previous results on the subject.

The most important outcome here is clearly the occurrence of significant heterogeneities in the soil physical properties due to the suffusion process, as highlighted by the spatial maps of void ratio, inter-granular void ratio and fines content. More precisely, the loss of fines is substantially higher at the periphery of the sample, suggesting some preferential flow paths. On the contrary, a roughly homogeneous suffusion process is observed along the flow direction, apart from the upper portion of the sample, at the interstitial flow inlet, and more marginally at the bottom of the sample. Interestingly, it also appears that, with greater erosion intensity, the loss of fines gets much more uniformly distributed within the sample, but without removing the radial heterogeneities previously induced at smaller flow rates. In the case studied in this paper, the heterogeneity of the sample was such that the part of the sample around its revolution axis was slightly denser after erosion than in the initial state, whereas it was looser in the peripheral zones. This result comes by considering the whole solid phase (fines and coarse grains). Now, if only the coarse granular skeleton is considered, only a global compaction is observed. However, as this compaction is slightly more pronounced on periphery than in the centre of the soil sample, the soil is somehow "pre-sheared" to accommodate these different volume changes in different zones. All these complex loading histories experienced by the soil during the suffusion development make rather difficult the interpretation of post-erosion mechanical test (as triaxial compression) and even more the assessment, a priori, of the mechanical properties related to post-erosion physical state.

From a more general perspective, the existence of such pronounced heterogeneities, or even of localized singularities, is prone to question usual interpretations of suffusion tests at sample scale, where the soil structure is implicitly assumed to be homogeneous and where the erosion process is consequently expected to be uniform at the local scale. The same holds for the triaxial test, or other mechanical tests on eroded soil samples, whose results are used to determine the impact of suffusion on mechanical strength and predict a possible degradation of the shear resistance performance. Furthermore, the fact that these heterogeneities are likely to be induced by preferential flow paths nearby rigid walls of the testing cell also questions the relevance of characterizing the materials behaviour with small-scale devices, having their own inherent edges, to be subsequently applied to large-scale situations with totally different boundary conditions.

Acknowledgements A funding provided by Provence-Alpes-Côte d'Azur region is gratefully acknowledged as well as a fruitful partnership with the engineering company SAFEGE. The support of Grenoble Alpes University through the project ERODE (AGIR program) is also acknowledged. We thank P. Charrier and R. Aboul Hosn from Laboratoire 3SR, L.-H. Luu and A. Wautier from Irstea for the help provided during the realization of the tests presented in this paper. We also would like to thank Professors D. Marot and Y. Khidas for their fruitful discussions.

References

1. Benahmed N, Canou J, Dupla J-C (2004) Structure initiale et propriétés de liquéfaction statique d un sable. Comptes rendus mécanique 332(11):887–894
2. Bendahmane F, Marot D, Alexis A (2008) Experimental parametric study of suffusion and backward erosion. J Geotech Geoenviron Eng 134(1):57–67
3. Bianchi F et al (2018) Tomographic study of internal erosion of particle flows in porous media. Transp Porous Media 122(1):169–184
4. Bonelli S (2013) Erosion in geomechanics applied to dams and levees. Wiley, New York
5. Burenkova V (1993) Assessment of suffusion in non-cohesive and graded soils, in filters in geotechnical and hydraulic engineering. Balkema, Rotterdam, pp 357–360
6. Chang D, Zhang L (2011) A stress-controlled erosion apparatus for studying internal erosion in soils. Geotech Test J 34(6):579–589
7. Desrues J et al (1996) Void ratio evolution inside shear bands in triaxial sand specimens studied by computed tomography. Géotechnique 46(3):529–546
8. Dumberry K, Duhaime F, Ethier YA (2017) Erosion monitoring during core overtopping using a laboratory model with digital image correlation and X-ray microcomputed tomography. Can Geotech J 55(2):234–245
9. Fell R, Fry J-J (2014) Internal erosion of dams and their foundations: selected and reviewed papers from the workshop on internal erosion and piping of dams and their foundations, Aussois, France, 25–27 April 2005. CRC Press
10. Fonseca J et al (2014) Microstructural analysis of sands with varying degrees of internal stability. Géotechnique 64(5):405–411
11. Frost J, Park J (2003) A critical assessment of the moist tamping technique. Geotech Test J 26(1):57–70
12. Hall S et al (2010) Discrete and continuum analysis of localised deformation in sand using X-ray [mu] CT and volumetric digital image correlation. Géotechnique 60(5):315
13. Hasan A, Alshibli K (2010) Experimental assessment of 3D particle-to-particle interaction within sheared sand using synchrotron microtomography. Géotechnique 60(5):369
14. Homberg U et al (2012) Automatic extraction and analysis of realistic pore structures from ct data for pore space characterization of graded soil. In: Proceedings of 6th international conference on scour and erosion (ICSE-6). SHF, Paris, France, pp 345–352
15. Aboul Hosn R et al (2017) Microscale analysis of the effect of suffusion on soil mechanical properties. 11th International Workshop on Bifurcation and Degradation in Geomaterials (IWBDG 2017), May 21-25, 2017, Limassol, Cyprus. In: International workshop on bifurcation and degradation in geomaterials. Springer, Berlin
16. Aboul Hosn R et al (2018) Effects of Suffusion on the Soil's Mechanical Behavior: Experimental Investigations. 26th Annual Meeting of European Working Group on Internal Erosion EWG-

EI, 10-13 September 2018, Milano, Italy. Springer, Internal Erosion in Earthdams, Dikes and Levees - Proceedings of EWG-IE 26th Annual Meeting 2018, pp 3–15, 2018
17. Indraratna B, Raut AK, Khabbaz H (2007) Constriction-based retention criterion for granular filter design. J Geotech Geoenviron Eng 133(3):266–276
18. Israr J, Indraratna B, Rujikiatkamjorn C (2016) Laboratory investigation of the seepage induced response of granular soils under static and cyclic loading. Geotech Test J 39(5):795–812
19. Ke L, Takahashi A (2014) Triaxial erosion test for evaluation of mechanical consequences of internal erosion. Geotech Test J 37(2):347–364
20. Kenney T, Lau D (1985) Internal stability of granular filters. Can Geotech J 22(2):215–225
21. Kenney T, Lau D (1986) Internal stability of granular filters: reply. Can Geotech J 23(3):420–423
22. Kézdi Á (1979) Soil physics: selected topics (Vol. 25). Elsevier.
23. Li M, Fannin RJ (2008) Comparison of two criteria for internal stability of granular soil. Can Geotech J 45(9):1303–1309
24. Luo Y-L et al (2013) Hydro-mechanical experiments on suffusion under long-term large hydraulic heads. Nat Hazards 65(3):1361–1377
25. Marot D, Bendahmane F, Nguyen HH (2012) Influence of angularity of coarse fraction grains on internal erosion process. La Houille Blanche 6:47–53
26. Mehdizadeh A, Disfani M (2018) Micro scale study of internal erosion using 3D X-ray tomography. The 9th International Conference on Scour and Erosion, Taipei, Taiwan
27. Moffat R, Fannin RJ (2011) A hydromechanical relation governing internal stability of cohesionless soil. Can Geotech J 48(3):413–424
28. Moffat R, Fannin RJ, Garner SJ (2011) Spatial and temporal progression of internal erosion in cohesionless soil. Can Geotech J 48(3):399–412
29. Moraci N, Mandaglio MC, Ielo D (2011) A new theoretical method to evaluate the internal stability of granular soils. Can Geotech J 49(1):45–58
30. Sail Y et al (2011) Suffusion tests on cohesionless granular matter: experimental study. Eur J Environ Civ Eng 15(5):799–817
31. Scheuermann A, Kiefer J (2010) Internal erosion of granular materials–identification of erodible fine particles as a basis for numerical calculations. In: 9th International congress of the Hellenic society of theoretical and applied mechanics (HSTAM). Hellenic Society for Theoretical & Applied Mechanics (HSTAM)
32. Skempton A, Brogan J (1994) Experiments on piping in sandy gravels. Geotechnique 44(3):449–460
33. To P, Scheuermann A, Williams D (2018) Quick assessment on susceptibility to suffusion of continuously graded soils by curvature of particle size distribution. Acta Geotech 13(5):1241–1248
34. Tudisco E et al (2017) TomoWarp2: a local digital volume correlation code. SoftwareX 6:267–270
35. Wan CF, Fell R (2008) Assessing the potential of internal instability and suffusion in embankment dams and their foundations. Journal of geotechnical and geoenvironmental engineering, 134(3), 401–407
36. Xiao M, Shwiyhat N (2012) Experimental investigation of the effects of suffusion on physical and geomechanic characteristics of sandy soils. Geotech Test J 35(6):890–900